Advanced Engineering Informatics 58 (2023) 102235

Contents lists available at ScienceDirect

Advanced Engineering Informatics

journal homepage: www.elsevier.com/locate/aei

Full length article

Prediction of railroad track geometry change using a hybrid CNN-LSTM spatial-temporal model

Xin Wang [a], Yun Bai [b,*], Xiang Liu [a]

[a] Department of Civil and Environmental Engineering, Rutgers, The State University of New Jersey, Piscataway, New Jersey, USA
[b] Intelligent Transportation Thrust, Hong Kong University of Science and Technology (Guangzhou), Guangdong, China

ARTICLE INFO

Keywords:
Track geometry prediction
Positional error correction
Spatial-temporal dependence
CNN-LSTM

ABSTRACT

Track geometry is highly important for ensuring railroad safety. Predicting track geometry degradation can support preventive maintenance by identifying and prioritizing track segments that are more prone to potential track geometry defects. This paper develops a novel machine learning approach that can simultaneously geospatially align track geometry data from multiple inspections accounting for positional errors, and also predict foot-by-foot track geometry change over time. The proposed position correction method considers multiple geometry parameters to provide highly accurate positional information for geometry measurements, which is a prerequisite for foot-by-foot track geometry prediction. A hybrid CNN (convolutional neural network)-LSTM (long short-term memory neural network) machine learning model is developed to account for spatial–temporal dependence with respect to foot-by-foot track geometry change. Specifically, CNN is used to incorporate spatial dependence of track geometry on adjacent segments. LSTM is applied to learn dynamic changes in track geometry data over time to consider the temporal dependence. The hybrid CNN-LSTM model is validated using track inspection data provided by one major freight railroad in the United States. The results show that our positional error correction method can reduce the relative positional error to less than 1 foot with a 99% confidence interval. Our proposed CNN-LSTM model outperforms four other models, including a naïve model (using the last observation), multi-layer perceptron (MLP), plain CNN, and plain LSTM, for both short-term and long-term prediction periods. The proposed hybrid machine learning methodology can be adapted to various other freight and passenger rail lines. The predictive track geometry change information can be used by the industry to plan and prioritize resources for preventative maintenance, yielding benefits in safety and operational efficiency.

1. Introduction

Track geometry is one of the most important factors in rail infrastructure management and maintenance [1,2]. Track geometry degradation can lead to significant increases in the dynamic loads between rails and wheels, decreasing track service life and jeopardizing rail transportation. According to the Federal Railroad Administration (FRA) rail equipment accident database, track geometry defects are the second largest cause of freight-train derailments in the United States [3], following broken rails. Accurate track geometry prediction can assist maintenance staff in preventive maintenance that aims to improve the safety and sustainability of freight rail service. In this way, rail transportation safety can be enhanced alongside an increase in economic competitiveness within the industry.

Autonomous track assessment cars (ATACs) travel in revenue service, measuring track geometry including profile, alignment, gauge, crosslevel, and warp (Fig. 1). The track geometry data are sampled at 1-foot intervals. To improve the inspection quality, concrete is added to increase the weight of the ATACs (to 110 tons total) [4].

Modeling and predicting track geometry have been key parts of the advanced railroad management system and are important for predictive maintenance and capital planning [5,6]. However, accurate foot-by-foot track geometry prediction has been challenging due to issues of positional error (offset) and complex temporal and spatial dependence:

(1) **Positional error**: The offset between two geometry measurements has been extensively studied in previous research to provide high-quality geometry data for track condition evaluation

* Corresponding author.
E-mail address: yunbai@hkust-gz.edu.cn (Y. Bai).

https://doi.org/10.1016/j.aei.2023.102235
Received 10 May 2023; Received in revised form 12 October 2023; Accepted 20 October 2023
Available online 3 November 2023

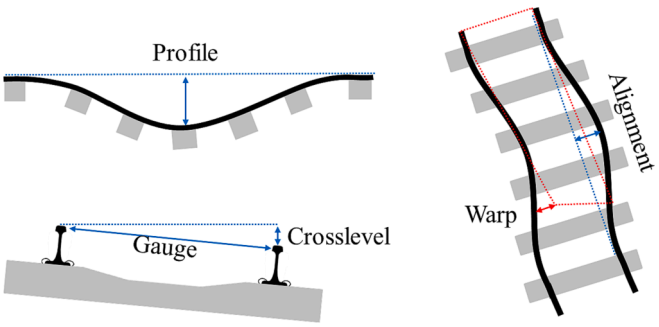

Fig. 1. Schematic Diagrams of Some Track Geometry Characteristics.

and prediction [7,8]. These studies also indicate that highly accurate positional information is essential for microscale track condition analysis, such as foot-by-foot track geometry prediction.

(2) **Temporal dependence**: Generally, track segments with greater geometry amplitudes tend to experience significantly higher dynamic loads between wheel and rail, leading to faster degradation. Track geometry changes dynamically over time due to the influence of traffic [9–12], curve [13], grade [14], track class/speed [15,16], and other factors [17,18].

(3) **Spatial dependence**: Track geometry of adjacent track segments might be correlated and has similar degradation patterns. The infrastructure (e.g., curve and grade) and substructure condition (e.g., settlement, fouling level, and drainage properties) of adjacent segments are correlated, resulting in similar geometry amplitude and degradation patterns [19]. However, spatial dependence in track geometry has not yet been investigated in previous studies. To this end, this paper introduces a method to evaluate the spatial dependence of geometry amplitude and degradation, as shown in Fig. 2(a). The spatial correlation of geometry amplitude is calculated by comparing two geometry measurements with different offsets. To determine the spatial correlation of geometry degradation, the change in amplitude is first generated by taking the difference between two measurements. Subsequently, the correlation is given based on the degradation amplitudes and lagged (shift) copies of the values. The correlation results (Fig. 2(b)) indicate that both geometry amplitude and geometry change (degradation) are spatially correlated with the values on adjacent track segments, especially for geometry amplitudes.

The issues described above make it challenging to accurately predict foot-by-foot track geometry measurements. First, accurate positional information is a prerequisite for predicting foot-by-foot track geometry. A novel data alignment method is proposed to provide highly accurate relative positional information to align multiple geometry measurement data. Some new issues in geometry measurements have been found to be associated with the data collected by inspection vehicles approaching from two directions (see Section 4.1.1), and an algorithm for data alignment needs to be developed to handle geometry data with these issues. The second challenge is predicting the geometry over a short segment because of the complex spatial–temporal dependence. This means that the dynamic changes of geometry over time (temporal dependence) and the inter-segment degradation correlation (spatial dependence) must be taken into account. In this paper, we develop a novel hybrid machine learning method to capture the spatial–temporal dependence of track geometry to achieve highly accurate predictions.

2. Literature review

Data alignment (synchronization) is a crucial component of analyzing time series data in order to identify variations and common patterns across individual signals [20,21]. In railway engineering, positional error is a common issue associated with geometry measurement, which is caused by radius errors of the rolling wheel [22,23], wheel/rail contact condition (e.g., slip and slide) [24], and calibration frequency of the measurement system [25,26]. Positional errors can be divided into two categories: (1) absolute positional error, and (2) relative positional error. Absolute positional error refers to the difference between the positional information inspected and the actual location. Relative positional error refers to the difference of positional information between multiple measurements [27]. The absolute positional information is important for maintenance workers to locate the geometry defects on the track that are detected during inspection. To correct absolute error, physical positional devices including global positioning system (GPS) [26,28–31], differential global positioning system (DGPS) [32], and radio frequency identification (RFID) [33] are applied during the inspection process. Algorithms were proposed to match the characteristics of track equipment (i.e., curves and turnouts) during the inspection and to correct the absolute positional error using actual positional information [27,34].

On the other hand, accurate relative positional information is needed for track degradation analysis, especially for foot-by-foot track geometry degradation predictions. Most researchers manually selected one previous inspection dataset as their reference file for aligning the current inspection data. The least square method is a commonly used alignment

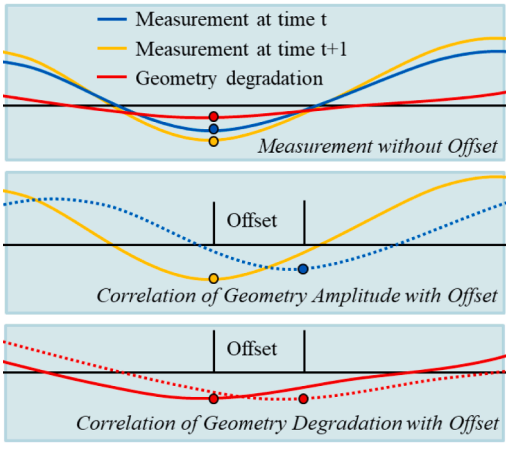

(a) Illustration of Calculation Process

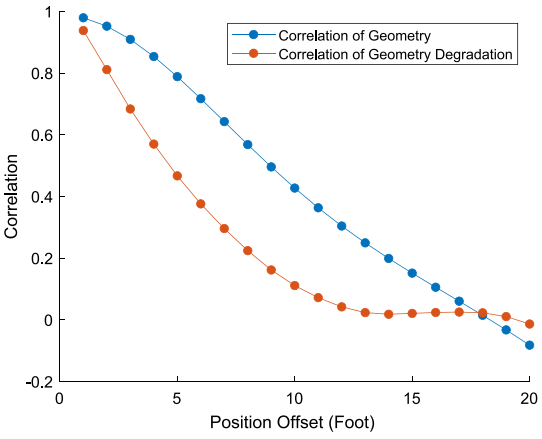

(b) Correlation Results

Fig. 2. Correlation of Geometry Measurements Under Different Offsets.

method that compares the total sum of squares of signals to determine offsets [35,36]. Cross-correlation coefficient was also applied to measure the similarity and determine the lag that maximizes the correlation between the two signals [37]. Dynamic time warping (DTW) and extension of DTW (i.e., variable penalty DTW) utilize a distance matrix and a warping path to align datasets in different fields including track geometry alignment [38] and spoken word processing [39].

However, the aforementioned models are subject to outliers in the inspection data. The position of geometry data could be falsely corrected if the selected geometry parameter included multiple outliers [8]. Correlation optimized warping (COW) divides the signals into smaller segments of equal length and aligns corresponding segments by stretching or compressing them, which can reduce the impact of outliers on the alignment process [40]. Similarly, partial linear fit [41], interval correlated shifting [42], and peak alignment by Fast Fourier Transform [43] align datasets based on local correlation by splitting the dataset into equal segments. To take both local and global correlations into consideration, hierarchical cluster-based peak algorithm [44] and segment-wise peak alignment were developed [45]. Furthermore, Wang et al. [8] proposed a more robust position synchronization model by considering multiple parameters of geometry information in high-speed railroads, which could reduce the miscorrection of positional errors even if one geometry parameter data had multiple outliers or missing values. Recently, a combined method based on recursive alignment by fast fourier transform and correlative optimized warping was applied to improve the alignment precision of different inspection measurement data [7]. The positional errors of single track geometry defects could be reduced to below 0.25 m. Nevertheless, when dealing with geometry data collected by inspection vehicles approaching from two directions, new challenges arise, such as rail sides and data sign contradictions, which have not been addressed in previous studies.

Predictive maintenance for railroads using data-driven models leverages the prediction of infrastructure and rolling stock deterioration to proactively schedule maintenance activities [5,46]. They are crucial for maintaining the reliability and functionality of infrastructure and rolling stock to ensure the safety and efficiency of rail transportation and to avoid service disruptions [47]. Track geometry prediction has been one of the most important aspects in this context, as geometry can significantly impact the service life of both infrastructure and rolling stock. The degradation process of track geometry is subject to dynamic changes influenced by varying operation conditions (e.g., traffic volume and speed) and track components (e.g., grade and curve), which requires massive dynamic and static datasets from different sources to accurately predict the changes over time.

Extensive data-driven models have been developed in the field of track geometry prediction. Earlier prediction of TQI (Track Quality Index) can be found in Hamid and Gross [13], wherein they used a stepwise regression model considering previous TQI and physical parameters such as tonnage and speed. Other statistical methods, including linear function [48], exponential function [18], multi-stage linear model [49], piecewise linear regression model [50,51], autoregressive (AR) model [52], and autoregressive moving average (ARMA) method [53], have been applied to predict track geometry over a defined track section, such as 200-meter track section. Some other researchers have considered stochastic modeling techniques to characterize track geometry degradation, with Gaussian random process [54], bivariate Gamma process [55], Markov chain model [56] being explored. Furthermore, a survival model, a brunch of stochastic models, was developed to study the degradation of geometry defects and to model derailment risk as a function of track conditions [57]. The methods mentioned above are parametric as they rely on predefined functional forms and assumptions about the data distribution, which limits the flexibility and scalability of models in capturing complex relationships in the data.

With the development of big data and artificial intelligence, non-parametric machine learning models have been proposed and employed in recent years to predict track geometry degradation, including random forests (RF), support vector machine (SVM), and artificial neural networks (ANNs). For example, RF was used to predict the future track deterioration index that was calculated based on the standard deviation of track geometry parameters [58]. Hu and Liu [15] elaborated SVM to predict both the change in track geometry defect amplitude, and when a yellow tag defect might grow large and become a red tag defect. Later, Lasisi and Attoh-Okine [59] applied the SVM model to predict deviation from the predefined TQI threshold and found that SVM outperformed the RF for the studied dataset. Multi-layer perceptron (MLP) consists of multiple layers of neurons where each is fully connected to those in the layers below and above [60]. MLP was applied to predict the track geometry deterioration rate [61] and geometry change in terms of TQI [16] over a track section. Three types of models, RF, SVM, and MLP, were employed to predict the track degradation index (a mixture of geometry deviations) for a tram network using vehicle acceleration data [62]. They found that RF made more accurate predictions compared to the other developed models (i.e., SVM and MLP) [62]. However, the aforementioned studies can only be used to predict the track geometry over a long track section and could not provide accurate predictions over short segments (foot-level) because of the ignorance of spatial dependence of geometry.

In addition to MLP, other common neural networks are the convolutional neural network (CNN) and recurrent neural networks (RNN). CNN has been widely used to acquire spatial dependence in image recognition [63], audio [64], and text [65]. RNN improves prediction accuracy iteratively by incorporating the previous output as an additional input [66]. Thus, RNN is particularly suited for applications with sequential data, and is able to consider the temporal dependence, such as track circuit fault diagnosis [67] and text mining [68]. However, CNN or RNN considered only one type of data characteristic (spatial or temporal feature) in their analysis. To overcome this limitation, the graph convolutional network (GCN) was applied to consider the spatial and temporal dependence of data with a complex graph structure including trafffic flow prediction [69] and clash change component prediction [70].

On the other hand, the railroad is a linear engineering infrastructure. CNN is able to perform convolution operations to consider the spatial effect from adjacent track segments, which is similar to acquiring spatial dependence in image recognition. To this end, the hybrid neural network, CNN-RNN, has shown its powerful capacity for feature extraction by taking advantage of both CNN and RNN. It has demonstrated its superior performance in multiple applications such as the prediction of vehicle-body vibration [71], patent risk prediction [72], and residential assistance [73]. Nevertheless, traditional RNN models often suffer from the vanishing gradient problem, which hinders their ability to learn long-term dependence in the data. In contrast, LSTM is an improved form of RNN, which introduces memory blocks instead of conventional simple RNN units to handle the problem of vanishing and exploding gradient [74–76]. LSTM algorithm learns long-term dependence between time steps in time series and sequence data. In other words, LSTM provides better capability in handling long sequences and capturing the temporal dependence in the data. In summary, by combining the strengths of both CNN and LSTM, the hybrid network could extract both spatial and temporal features from data in a more robust and effective way. This demonstrates the potential of the CNN-LSTM approach for analyzing track geometry data.

3. Knowledge gap and intended contribution

Many studies have been conducted to handle the offset between multiple geometry measurements [7,8,35–38]. Multiple geometry parameters were considered to provide a robust estimation of the positional errors for passenger railroads [8]. However, for geometry data collected by inspection vehicles approaching from two directions, issues including rail sides and data sign contradiction would occur, and have not been considered in previous studies. Therefore, a customized

algorithm is needed to properly handle geometry data with this issue.

Furthermore, there are many existing geometry prediction methods that consider temporal dependence, including linear function [48], exponential function [18], stepwise autoregression model [13], SVM [15], RF [58], and MLP [16,62]. While those methods consider the dynamic change of track geometry, they do not account for the spatial dependence of track geometry degradation over a short track segment, especially for foot-by-foot track geometry prediction.

Considering the limitations of prior studies, this paper develops a spatial–temporal approach for predicting foot-by-foot track geometry measurement by considering spatial and temporal dependence based on the aligned track geometry data after automatically correcting positional errors. Our specific research tasks are as follows. First, this research proposes an algorithm for aligning multiple geometry measurements collected by vehicles approaching from two directions. Then, based on the processed data and other related data (i.e., traffic, speed, grade, and curvature), a spatial–temporal model, CNN (convolutional neural network) -LSTM (long short-term memory neural network), is developed to predict the foot-by-foot geometry measurement. This can assist maintenance staff in preventive maintenance and proactive planning that aim to improve the safety and sustainability of rail service. This paper provides the following key contributions:

1. A spatial–temporal model, CNN-LSTM, is proposed to effectively capture spatial and temporal information from data.
2. A case study has been conducted based on track inspection data from Class I U.S freight railroad mainlines to demonstrate the feasibility of the proposed approach for practice in the industry. To the best of our knowledge, this is the first time that both spatial and temporal dependence have been simultaneously considered in foot-by-foot track geometry prediction on railroads. CNN is employed to extract the spatial features from different track segments as inputs. Based on the obtained time series data with spatial features, the LSTM model was applied to capture temporal patterns and predict the dynamic changes in geometry.
3. Multi-source data including historical geometry measurements, traffic, speed, grade, and curvature are included in the spatial–temporal model.
4. An algorithm for aligning the multiple track geometry measurements on railroads is customized to provide accurate relative positional information for geometry measurements.

4. Methodology

A novel spatial–temporal hybrid machine learning model is proposed in this paper to predict foot-by-foot track geometry on railroads. Fig. 3 illustrates the technical framework of the proposed research. The framework mainly consists of data preparation and spatial–temporal modeling for predicting track geometry.

Data preparation consists of three steps: positional error correction, data cleaning, and data integration. The method for aligning the relative position of track geometry data includes mapping rail sides and correcting relative positional errors. Then, data cleaning is applied to address the data issues including missing values and outliers. Data integration combines different databases related to geometry measurements, infrastructure data, and operation data according to positional information. Based on the processed data, a hybrid CNN-LSTM model is developed to predict foot-by-foot track geometry measurements by capturing both the spatial and temporal features. The following subsections present the proposed methodology in detail.

4.1. Data preparation

4.1.1. Positional error correction

Mapping Rail Sides

Typically, in high-speed railroad networks, trains travel in one direction on one track [8]. However, single track is commonly seen on freight railroads where track geometry inspection vehicles run in two directions on same track, as shown in Fig. 4. The first issue associated with geometry measurements from this kind of inspection is rail side contradiction. If one inspection vehicle (Vehicle 1) travels from left to right, the positional information in inspection files is recorded in ascending order. In this case, Rail 1 and Rail 2 are defined as left and right rail in the geometry measurement, respectively. However, when another inspection vehicle (Vehicle 2) runs from right to left, the positional information is in descending order. Rail 1 and Rail 2 are recorded

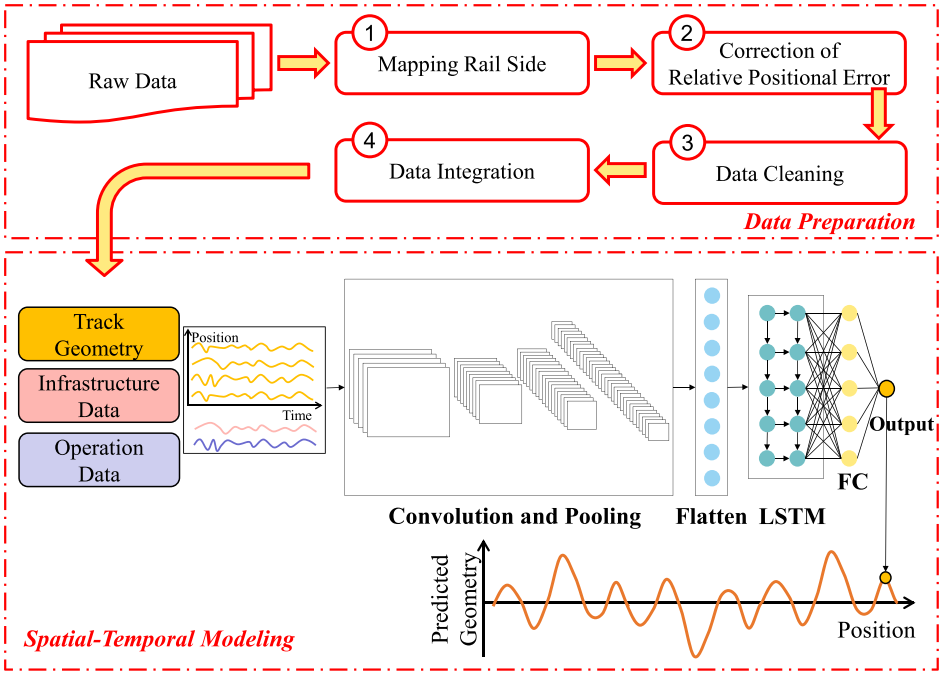

Fig. 3. The Framework of Positional Error Correction and Track Geometry Prediction.

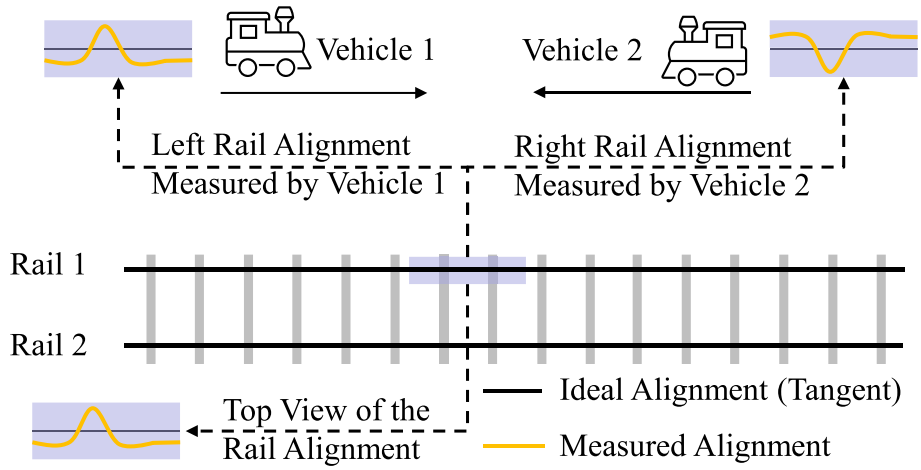

Fig. 4. Illustration of Geometry Inspection Car Movement from Two Directions on Railroads.

as right and left rail, respectively.

Furthermore, there is the sign (positive or negative values) contradiction issue. The alignment of Rail 1, for example, is offset to the left and is recorded as having positive amplitudes in the database collected by Vehicle 1. The same geometry would be recorded as being offset to the right, which is indicated as having negative values in the database from Vehicle 2.

To solve the issues caused by inspection vehicles running in opposite directions, geometry measurements with the positional information in ascending order are used as reference files to uniform geometry measurements. The detailed procedures for handling the geometry measurements collected from the other direction (data recorded in descending order) are presented in Table 1.

Correction of Relative Positional Error

Correcting the relative positional error refers to shifting the foot-by-foot position of geometry measurement data to the most likely position. Prior to this, it is important to estimate the positional error.

Suppose that there are two track geometry inspection runs at the time of i and j with track geometry measurement (e.g., profile) as X_i and X_j (Fig. 5), respectively. For a track segment, the geometry measurement from i and j inspections are:

$$X_i^{(k,l)} = \left\{ x_{in} | k - \frac{l}{2} < n < k + \frac{l}{2} \right\} \tag{1}$$

$$X_j^{(k,l)} = \left\{ x_{jn} | k - \frac{l}{2} < n < k + \frac{l}{2} \right\} \tag{2}$$

where k is the central point of the track segment and l is the segment length.

The relative positional error (offset) of segment k in i inspection with respect to j inspection (X_j is used as reference data) is δ_{ij}, which is defined as the distance to maximize the Pearson correlation coefficient r. The positional error δ_{ij} is calculated using Eq. (3).

$$\delta_{ij} = \underset{\delta}{\operatorname{argmax}} \left(r\left(X_i^{(k,l)}, X_j^{(k+\delta,l)} \right) \right) \tag{3}$$

Table 1
Procedures for Handling Geometry Measurement Collected from the Other Direction.

Geometry parameter	Switch the rail side	Change the sign
Left/Right rail profile	√	–
Left/Right rail alignment	√	√
Gauge	–	–
Crosslevel	–	√
Warp	–	√

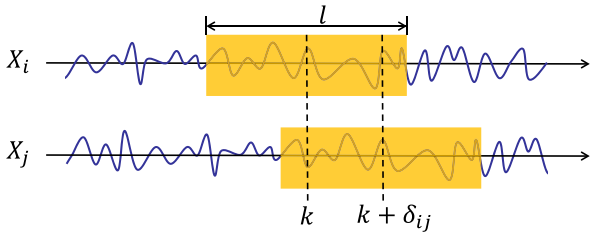

Fig. 5. Relative Positional Error Between Two Geometry Inspections.

$$r\left(X_i^{(k,l)}, X_j^{(k+\delta,l)} \right) = \frac{cov\left(X_i^{(k,l)}, X_j^{(k+\delta,l)} \right)}{\sigma X_i^{(k,l)} \bullet \sigma X_j^{(k+\delta,l)}} \tag{4}$$

Where σ is the standard deviation, and cov is the covariance of two vectors. In this case, the correlation coefficient ρ_{ij} is defined in Eq. (5).

$$\rho_{ij} = r\left(X_i^{(k,l)}, X_j^{(k+\delta_{ij},l)} \right) \tag{5}$$

When $m(i,j < m)$ inspection runs are conducted on the railroad, the relative positional error of segment k between two inspection files can be denoted using an overall error matrix E.

$$E = \begin{bmatrix} \delta_{11} & \cdots & \delta_{1m} \\ \vdots & \ddots & \vdots \\ \delta_{m1} & \cdots & \delta_{mm} \end{bmatrix} \tag{6}$$

The relative positional error can be falsely estimated due to the periodic geometry pattern and outliers in the geometry measurement. Therefore, three constraints are introduced to avoid the false estimation of relative error, as shown in Eq. (7).

First, the relative error should be limited to a given threshold δ_0, to avoid false mapping of the geometry measurements with periodic geometry patterns. Second, the correlation coefficient between geometry measurements at different times should be greater than threshold ρ_0 because they are highly correlated and have similar geometry patterns. Last, positional errors of adjacent track segments are similar, which means that the difference of positional errors between two adjacent track segments $\nabla\delta_{ij}$ should be limited to a given threshold δ_1.

$$s.t.: \begin{cases} \delta_{ij} \le \delta_0 \\ \rho_{ij} \ge \rho_0 \\ \nabla\delta_{ij} \le \delta_1 \end{cases} \tag{7}$$

Once the false estimation is identified using one geometry parameter, other geometry parameters are used for positional error correction. Prior to using other parameters, the positional errors between the different parameters are addressed using the method proposed by Wang et al. [8]. For example, the profile is used as the geometry parameter in positional error estimation. When the δ_{ij} is obtained using Eq. (3), and the constraints (Eq. (7)) are violated, the alignment will be used as the geometry parameters for positional error estimation. This process is iteratively performed until the correct error is determined. When the reliable estimation cannot be determined after leveraging all geometry parameters, δ_{ij} in E would be replaced with a missing value.

The most likely position is determined based on the assumption that the relative positional error of each pair of two files is randomly distributed. In other words, the summation of the distance from the measured positions to the most likely position is equal to zero. Additionally, the most likely position provides minimum difference from all measured positions. Therefore, the offset of a track segment between the position measured from i inspection to the most likely position θ_i^* can be determined by Eq. (8).

$$\begin{cases} \theta_i^* = arg\min_{\theta_i} \sum_{i=1}^{m}\sum_{j=1}^{m}\left(\delta_{ij}-\theta_i\right)^2 \\ \sum_{i=1}^{m}\theta_i = 0 \end{cases} \tag{8}$$

The augmented Lagrangian method is applied to solve the least squares problem with equality constraint by defining the Lagrangian function (Eq. (9)). It combines the objective function with a penalty term for constraint violations.

$$L = \sum_{i=1}^{m}\sum_{j=1}^{m}\left(\delta_{ij}-\theta_i\right)^2 + \lambda\sum_{i=1}^{m}\theta_i + \frac{\mu}{2}\sum_{i=1}^{m}\theta_i^2 \tag{9}$$

where λ is the Lagrange multiplier and μ is the penalty term.

The Lagrangian function L is minimized by computing the gradient of the function with respect to the variables δ_{ij} and θ_i, updating the estimates for the variables, and iteratively updating λ. If the constraint is satisfied, increase the value of μ. If the constraint is not satisfied, decrease the value of μ. This procedure is recursively repeated until the constraint is satisfied and the objective function is minimized to the desired tolerance. The most likely position θ_i^* can be estimated using Eq. (10).

$$\theta_i^* = \frac{1}{m}\sum_{i=1}^{m}\delta_{ij} - \frac{1}{m^2}\sum_{i=1}^{m}\sum_{j=1}^{m}\delta_{ij} \tag{10}$$

When δ_{ij} is identified as a false estimation, it is defined as a missing value. To consider the effect of false estimations, a binary variable b_{ij} is introduced to indicate if the relative positional error can satisfy the constraints, which is shown in Eq. (11). The number of reliable estimations m^* is calculated using Eq. (12).

$$b_{ij} = \begin{cases} 1, when \delta_{ij} \le \delta_0 \cap \rho_{ij} \ge \rho_0 \cap \nabla\delta_{ij} \le \delta_1 \\ 0, otherwise \end{cases} \tag{11}$$

$$m^* = \sum_{j=1}^{m} b_{ij} \tag{12}$$

Finally, the most likely position θ_i^* is defined by Eq. (13) with consideration of the false estimation.

$$\theta_i^* = \frac{1}{m^*}\sum_{i=1}^{m}\delta_{ij}b_{ij} - \frac{1}{m^{*2}}\sum_{i=1}^{m}\sum_{j=1}^{m}\delta_{ij}b_{ij} \tag{13}$$

After having offset for each track segment, the linear interpolation approach is applied to generate the positional information after correction.

4.1.2. Data cleaning

The previous section presents the algorithm that can provide a robust correction of positional error even with outliers in the raw geometry measurement data. However, data issues including outliers and missing values can still significantly affect the machine learning model and track geometry prediction. In this research, the change rate of each set of two adjacent track segments (one foot) is applied to identify the outliers in the geometry data. When the change rate is greater than a given threshold c, the geometry amplitude is defined as an outlier. For geometry data at location n inspected at time of i denoted by x_{in}, the criterion for identifying outliers is represented by Eq. (14).

$$|x_{in+1} - x_{in}| \le c \tag{14}$$

Once the outliers are detected using the criterion above, values from the nearest track segments are applied to replace these outliers as well as the missing values. In the studied railroad network, 0.15 % of data has outliers or missing values.

4.1.3. Data integration and splitting

Data integration is performed to integrate various datasets into one file. First, relevant features that impact the deterioration of track geometry are extracted to capture the key influencing factors identified in the literature review. Specifically, historical track geometry measurements, annual traffic density (in MGT), curve degree, maximum allowable speed for each track segment, and track grade are used as the input variables for the proposed model. Multiple geometry files (p in total) and other related datasets are collected, which are combined according to location information, as shown in Fig. 6. Prefix, Track Number (single or multiple tracks), Milepost, and Feet are used to unify each track segment (one row) in the integrated file.

Once the inputs and outputs of the model are in one integrated file, the entire dataset is divided into training, validation, and test data. The training and validation data are implemented to develop a machine learning model. The test data is used to evaluate the performance of the model at predicting unseen data. In this research, 60 %, 20 %, and 20 % of the entire dataset were split according to temporal order for model training, validation, and testing, respectively, which could avoid data leakage causing model overfitting.

4.2. Track geometry prediction

The data-driven approach proposed for foot-by-foot geometry prediction includes spatial dependence modeling and temporal dependence modeling. The proposed model was fit on training data and was ultimately evaluated based on test data. In the model development stage, a hybrid CNN-LSTM model was developed to simultaneously account for the spatial and temporal dependences of track geometry measurement. CNN was used to capture the spatial features with the historical geometry data from different track segments as inputs. Based on the obtained time series data with spatial features, the LSTM model was applied to extract temporal features and predict the dynamic changes in geometry. The predicted track geometry amplitudes were generated through a fully connected (FC) layer.

4.2.1. Spatial dependence modeling

The main building block of CNN is the convolution layer, a mathematical operation that performs vector inner product to merge different sets of information. In this way, CNN is able to consider spatial dependence by automatically extracting local spatial features from the inputs and combining the local features into higher-order features.

This research sets the threshold of correlation coefficient at 0.8 to determine the length of segments with spatial dependence. At a certain offset, if there exists a strong correlation (over 0.8) between two geometry measurements (or geometry degradation), it is considered to be spatially correlated. Fig. 2(b) indicates that the geometry degradation (i.

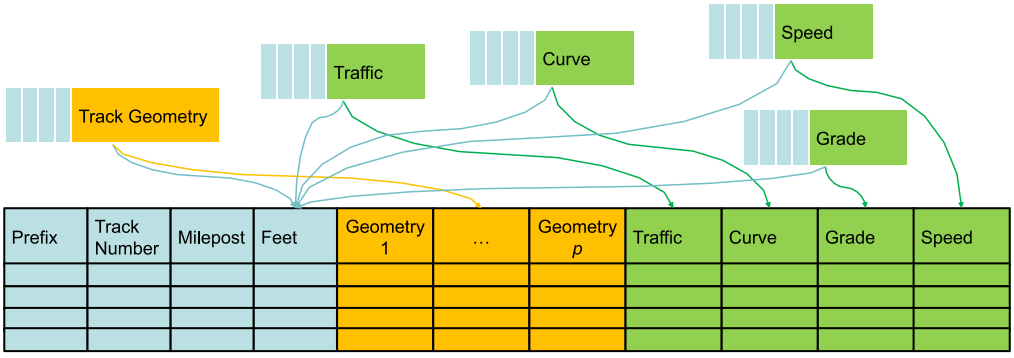

Fig. 6. Process of Data Integration for Various Datasets.

e., change of geometry amplitude) of a track segment is highly correlated with segments that are within two-foot offset. In terms of geometry amplitude, the offset of track segments with spatial dependence is extended to about 5 feet. In this research, the spatial features include geometry measurements within 5 feet of the central segment, allowing the consideration of spatial dependence of geometry degradation and amplitude.

As shown in Fig. 7, assuming that segment #6 is the central segment, the CNN model is applied to consider the spatial relationship between the central segment and its adjacent segments. In other words, the influence of historical geometry measurements from segment #1 to #11 are included to predict the future geometry amplitude of segment #6.

In addition to historical geometry measurements, other features associated with traffic, curve, speed, and grade are also included. They are defined as the constant values for each segment of interest. In total, there are 15 features considered in this research.

For a given training dataset $D = \{(I_i, y_i)|i = 1,2,\cdots,n\}$, I_i represents the input data. The prediction target y_i is a value indicating the geometry measurement at 1 ft over a future inspection run. n is the number of data samples. In the traditional models, each I_i indicates a 1-D vector containing temporal features. With the consideration of spatial dependence, in our proposed model, the input I_i is a 2-D matrix generated by Eq. (15).

$$I_i = concat(X_{pq}, T_{1q}, S_{1q}, C_{1q}, G_{1q}) \tag{15}$$

where $concat(\bullet)$ is the concatenate operation to integrate the matrix vertically. X_{pq} ($X_{pq} \in \mathbb{R}^{p\times q}$) is geometry measurements from p time steps and q positions. This research sets $p = 32$ due to data availability and $q = 11$ according to domain knowledge as the track segments within 5 feet exhibit high spatial correlation (Fig. 2(b)). T_{1q}, S_{1q}, C_{1q} and G_{1q} represent the traffic, speed, curve, and grade information, respectively, each consisting of a 1-D vector with dimensions of $1 \times q$. Thus, the input I_i ($I_i \in \mathbb{R}^{p\times q+4}$) includes both spatial and temporal features.

In CNN, the high-level feature representation is obtained by extracting the original feature I_i, as shown in Eq. (16).

$$A_i = f(\omega \bullet I_{i:i+g-1} + b_c) \tag{16}$$

where A_i denotes the output of the convolution layer; ω is the convolution kernel; $I_{i:i+g-1}$ is the i^{th} feature to the $(i+g-1)^{th}$ feature; g is the size of the convolution kernel; b_c is the bias term of the layer; and $f(\bullet)$ is the nonlinear activation function.

The pooling layer is introduced to reduce the size of the output feature by taking the maximum value within a sliding window. The output of the pooling layer is denoted by M and can be computed using Eq. (17).

$$M = \max(A_1, A_2, .., A_{p-g+1}) \tag{17}$$

There are four 2-D convolution layers adopted with rectified linear unit (Relu) as the activation function. More details about the hyperparameters of convolution layers are presented in Table 2.

The output of the last pooling layer is then flattened into a 1-D vector V using Eq. (18), which is utilized as input for the temporal dependence model (See section 4.2.2).

$$V = flatten(M) \tag{18}$$

where $flatten(\bullet)$ function is used to convert the multiple 2-D matrices to a 1-D vector V ($V \in \mathbb{R}^{6144\times 1}$ in this research). The flattened 1-D vector retains the information from the original 2-D matrices M but represents it in a single continuous sequence.

4.2.2. Temporal dependence modeling

By incorporating memory blocks, the LSTM algorithm can effectively capture and model long-term dependence between time steps in sequence data. An LSTM layer consists of the hidden state (aka. output state) and the cell state [77], as shown in Fig. 8(a). The hidden state contains the output of the LSTM layer for the current time step. The cell

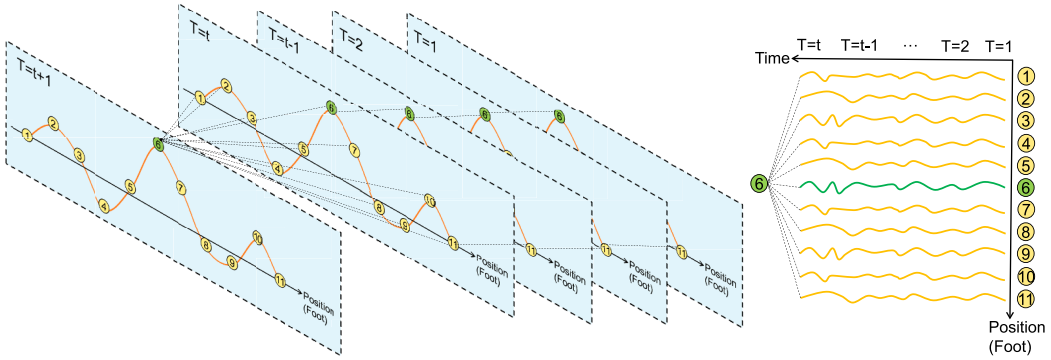

Fig. 7. Spatial Dependence of the Geometry Measurements.

Table 2
Hyper-parameter of the Spatial Dependence Model.

Layer	Input	Output	Kernel number	Kernel size	Batch normalization	Number of learnable parameters (Conv2D layer + batch normalization)
Input	15 × 32 × 1	15 × 32 × 1	–	–		–
Conv2D	15 × 32 × 1	15 × 32 × 32	32	4 × 4 × 1	Yes	544 + 64
Conv2D	15 × 32 × 32	7 × 16 × 64	64	4 × 4 × 1	Yes	32832 + 128
Conv2D	7 × 16 × 64	3 × 8 × 128	128	4 × 4 × 1	Yes	131,200 + 256
Conv2D	3 × 8 × 128	3 × 8 × 256	256	4 × 4 × 1	Yes	524,544 + 512
Flatten	3 × 8 × 256	6144 × 1	–	–		–

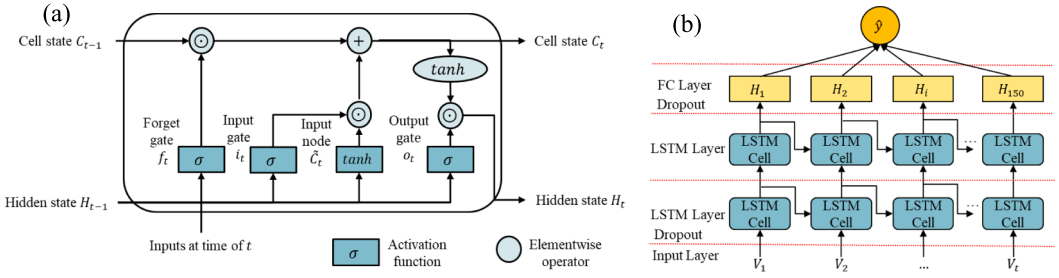

Fig. 8. Temporal Dependence Modeling (a). Process of Computing the Hidden State in LSTM Cell; (b). Structure of Temporal Dependence Model.

contains the information learned from the previous time step. At each time step, the LSTM layer adds or removes information from the cell state. It controls the flow of information using three multiplicative units: input gate, output gate, and forget gate.

In the previous phase, the spatial dependence model, CNN, generates the 1-D vector V with dimension of 6144 × 1. Subsequently, this vector is utilized as the input of the temporal dependence model, LSTM, to capture temporal patterns and dependence in the data (Fig. 8(b)). At time step t, the input gate (i_t), forget gate (f_t), and output gate (o_t) are calculated based on the hidden state at time step $t-1$ (H_{t-1}), using Eq. (19)–(21).

$$f_t = \sigma\left(W_{sf}H_{t-1} + W_{xf}V_t + b_f\right) \tag{19}$$

$$i_t = \sigma(W_{si}H_{t-1} + W_{xi}V_t + b_i) \tag{20}$$

$$o_t = \sigma(W_{so}H_{t-1} + W_{xo}V_t + b_o) \tag{21}$$

where, W_{sf}, W_{si}, W_{so}, W_{xf}, W_{xi}, and W_{xo} are learnable weight parameters. b_f, b_i, and b_o are learnable bias parameters. V_t denotes the data information at time step t from the 1-D vector V. σ is the sigmoid function in this research for computing the gate activation function. The cell state at time step t C_t is given by Eq. (22):

$$C_t = f_t \odot C_{t-1} + i_t \odot \widetilde{C}_t \tag{22}$$

where $\odot$ is the Hadamard product operator (element-wise multiplication of vectors). $\widetilde{C}_t$ is the input node using a *tanh* function with a value range of $(-1, 1)$ as activation function, which can be determined based on Eq. (23).

$$\widetilde{C}_t = tanh(W_{sc}S_{t-1} + W_{xc}V_t + b_c) \tag{23}$$

Where W_{sc} and W_{xc} are learnable weight parameters, and b_c is learnable bias parameter. Finally, the output of cell state C_t at time step t, i.e., the hidden state H_t, is calculated using Eq. (24).

$$H_t = o_t \odot tanh(C_t) \tag{24}$$

The input gate determines which relevant information can be added. The forget gate decides which relevant information from the prior steps is needed. The output gate finalizes the next hidden state of the neural network. For example, the output gate is always in the interval $(0, 1)$. When the output gate is close to 1, the cell state can impact the subsequent layers uninhibited, whereas for output gate values close to 0, the current cell state is prevented from impacting the other cell states.

This research uses two LSTM layers with 150 LSTM cells in each layer, as shown in Table 3. The "Dropout" is introduced between flatten layer and the first LSTM layer, and between the second LSTM layer and FC layer to randomly set their connection weights to zero to avoid overfitting. The probability of dropping out is set at 20 %. The final prediction result $\hat{y}_i$ of the spatial–temporal model is generated by converting the output of two-layer LSTM using the nonlinear activation function $f(\bullet)$, which is presented in Eq. (25).

$$\hat{y}_i = f(H_1, H_2, \cdots, H_{150}) \tag{25}$$

The proposed deep learning model, CNN-LSTM, has 4.6 million learnable parameters. Furthermore, multi-step prediction of geometry is used to provide long-term prediction results to assist with predictive maintenance and capital planning. This method entails predicting the subsequent geometry in a sequence using results predicted in previous steps as inputs.

4.2.3. Loss function and evaluation metrics

In the training process, the goal is to minimize the difference between the actual geometry amplitudes and the predicted values. The loss function of the CNN-LSTM model is shown in Eq. (26).

$$\mathscr{L} = \frac{1}{n}\sum_{i=1}^{n}(y_i - \hat{y}_i)^2 \tag{26}$$

where n is the number of instances, y_i indicates the actual geometry

Table 3
Hyper-parameters of the Temporal Dependence Model.

Layer	Input	Output	Dropout	Number of learnable parameters
LSTM	6144 × 1	150 × 1	Between flatten layer and the first LSTM layer	3,777,000
LSTM	150 × 1	150 × 1	–	180,600
FC	150 × 1	1 × 1	Between the second LSTM layer and FC layer	151
Output	–	1 × 1	–	–

value, and $\hat{y}_i$ denotes the predicted result. Evaluation metrics are measures for indicating the performance of the proposed model. Root mean square error (RMSE) is a widely used metric for comparing the difference between values predicted by a model and actual values, which is defined in Eq. (27).

$$RMSE = \sqrt{\frac{1}{n}\sum_{i=1}^{n}(y_i - \hat{y}_i)^2} \tag{27}$$

The mean absolute percentage error (MAPE) is another metric commonly used to measure the accuracy of a model, and is calculated by Eq. (28).

$$MAPE = \frac{100}{n}\sum_{i=1}^{n}\left|\frac{y_i - \hat{y}_i}{y_i}\right| \tag{28}$$

However, it can be deceptive when the actual geometry value is close to zero [78]. The weighted mean absolute percentage error (WMAPE) is proposed to overcome the shortage of MAPE, which is defined using Eq. (29).

$$WMAPE = \frac{100}{n}\frac{\sum_{i=1}^{n}|y_i - \hat{y}_i|}{\sum_{i=1}^{n}|y_i|} \tag{29}$$

In this research, both RMSE and WMAPE are applied to evaluate the performance of the prediction model.

5. Case study

5.1. Data overview

Data pertaining to this study were collected from one major Class I U. S freight railroad. The data came from the inspection of around 80 miles of track on this railroad. There are three types of data used in this case study: track geometry data, infrastructure data, and operation data. The following sections present the details of the railroad data.

Track geometry describes the surface of the track based on multiple geometric parameters including profile, alignment, gauge, crosslevel, and warp. In the studied railroad network, track geometry for each foot is inspected by automated track inspection vehicles twice per week. This research's data includes 61 geometry measurements collected over 8 months of inspection.

Infrastructure data contains curve data and grade (slope) data. The curve data includes the curve degree, curve length, superelevation, and curve direction, which indicates the horizontal alignment of the track. Grade data provides the percentage of track slope, showing the vertical alignment of the track.

Operation data includes traffic data and speed data. Traffic data specifies the track segments and corresponding annual tonnage density (MGT). Speed data presents the maximum allowable speed for track segments.

5.2. Positional error correction

The aforementioned method (Section 4.1.1) was applied to obtain the relative positional error δ (Eq. Eq. (3)), correlation coefficient ρ (Eq. (5)), and the difference of positional errors between each set of two adjacent segments $\nabla\delta$, shown in Fig. 9. In this research, the threshold of δ, ρ, and $\nabla\delta$ were determined according to the 99 % confidence level, and were 14 *ft*, 0.82, and 8 *ft*, respectively.

The thresholds above were applied to identify false estimations of the positional error. Then, all the reliable estimations were used to correct the positional error. The comparison of track geometry data before and after positional error correction is shown in Fig. 10. Fig. 10(a) presents the raw left rail profile data from inspection runs. Confusion regarding rail side can be seen where the left rail profile data actually contains information from both the left and right rails, resulting from inspection vehicles traveling in two directions. Fig. 10(b) shows the data after mapping the rail side. At this step, the issue of mismatched rail side is solved. Fig. 10(c) indicates the geometry data after the positional error correction. At a 99 % confidence level, the positional error between multiple geometry measurements is reduced from 14 feet to less than 1 foot.

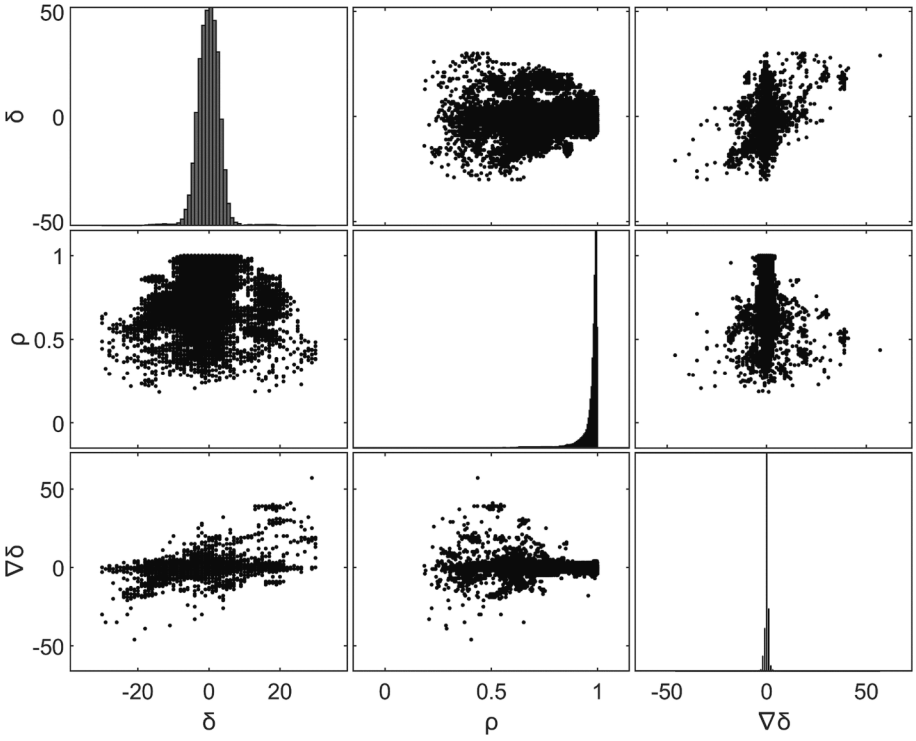

Fig. 9. Statistical Distribution of δ, ρ, and $\nabla\delta$.

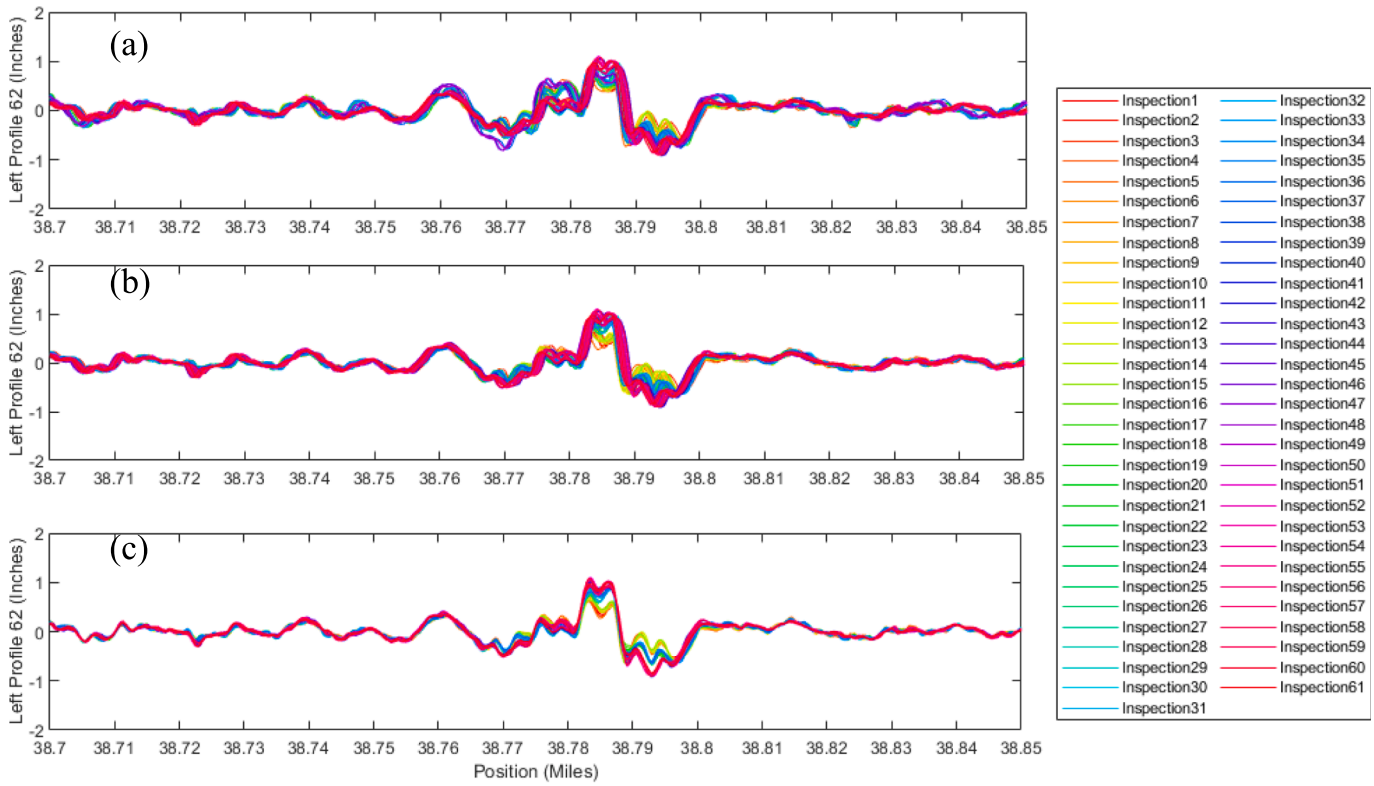

Fig. 10. Performance of Positional Error Correction (a) Raw Left Rail Profile Data from Inspection Runs, (b) Data After Mapping the Rail Side, (c) Data After Positional Error Correction.

5.3. *Prediction of track geometry*

The spatial–temporal model is trained on the training and validation dataset. In the training process, we set the learning rate to 0.001, the batch size to 64, and the training epoch to 1,500. The training and validation loss curves of the CNN-LSTM model are presented in Fig. 11. It indicates that the validation loss curve remains stable when the training epoch reaches around 1,300. Then, the trained CNN-LSTM model is applied to predict the geometry in the test dataset. The RMSE and WMAPE are calculated based on test dataset (12 measurements) accounting for 20 % of total dataset to evaluate the performance of the proposed model.

To compare their performance, the MLP, plain CNN, and plain LSTM models are separately developed. MLP has five hidden layers, and the numbers of hidden neurons for each hidden layer are 100, 100, 200, 100, and 100, respectively. The Relu function is used as the activation function for the hidden layers. The CNN and LSTM models apply the same hyper-parameters, as shown in Table 2 and Table 3. These three models are trained and tested based on the same training, validation, and test datasets. A naïve model is also employed by simply using the last observation of geometry amplitude for both short-term and long-term predictions. Furthermore, using multi-step prediction method, five models including the naïve model, MLP, CNN, LSTM, and CNN-LSTM are applied to predict track geometry over different timespans. In other words, it involves sequential prediction of subsequent geometry based on the same trained models by using previously predicted results as inputs. The relative performance of different methods is presented in Table 4.

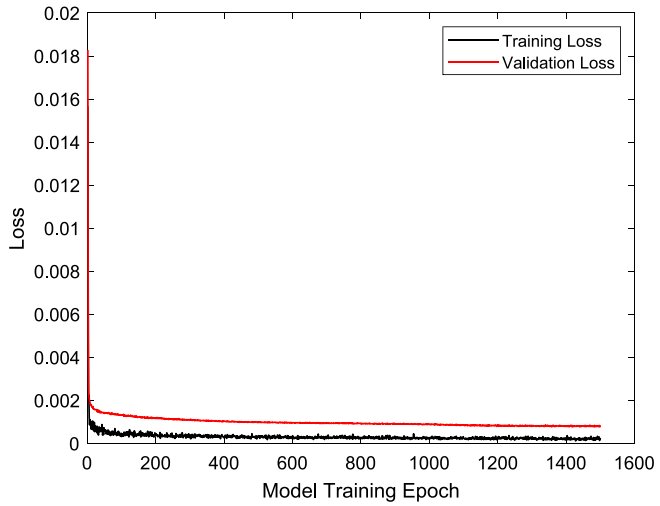

Fig. 11. Loss Curve of Training and Validation Dataset.

It is observed that the performance of all five models decreases when they are applied for predicting track geometry over a longer term period (e.g., two months in advance), as compared to short-term prediction (e.g., one week in advance). This is because, for multi-step prediction, the predicted geometry values will be directly used as inputs for the next prediction, which results in the accumulation of errors. In addition, it indicates that the CNN-LSTM model outperforms the other four models (i.e., naïve model, MLP, CNN, and LSTM), both at short-term (one week) and long-term prediction. The CNN-LSTM model has RMSE of 0.0093, with WMAPE of 4.51 % for one-week prediction. The RMSE and WMAPE increase to 0.0119 and 8.41 %, respectively, when the CNN-LSTM model is applied to predict geometry amplitudes two months in advance. These results also demonstrate the capability of LSTM in capturing temporal dependence in the geometry data as the plain LSTM has the second-best WMAPE of 11.34 % for two-month prediction. Although CNN alone may not provide accurate prediction results as effectively as LSTM, the integration of LSTM leads to a significant improvement. Specifically, the WMAPE of CNN reduces from 20.14 % to 8.41 % for a two-month prediction when LSTM is incorporated.

Table 4
Performance Comparison of the Different Approaches.

Time	Evaluation metric	Proposed model				
		Naïve model	MLP	CNN	LSTM	CNN-LSTM
1 week	RMSE (inches)	0.0958	0.0153	0.0241	0.0124	**0.0093**
	WMAPE	14.40 %	9.80 %	12.64 %	7.86 %	**4.51 %**
1 month	RMSE (inches)	0.1940	0.0177	0.0303	0.0159	**0.0105**
	WMAPE	21.65 %	11.19 %	17.88 %	9.98 %	**6.66 %**
2 months	RMSE (inches)	0.3150	0.0196	0.0349	0.0181	**0.0119**
	WMAPE	29.48 %	12.05 %	20.14 %	11.34 %	**8.41 %**

On the other hand, naïve model yields the worst prediction results compared to the other four models. Notably, the RMSE values of the naïve model are substantially higher, while WMAPE values are relatively higher. It suggests that the overall percentage error in the predictions is low, but individual errors can be quite significant in magnitude. In other words, naïve model cannot capture the degradation pattern of geometry for track sections having large geometry amplitude, especially for longer-term predictions.

The results above also demonstrate the significance of accounting for spatial–temporal dependence in track geometry prediction. The CNN-LSTM model allows for the consideration of historical geometry measurements as well as surrounding conditions of the segment of interest. From an engineering perspective, the dynamic changes of the track geometry are affected by geometry amplitude and historical degradation of the track segment of interest, which can be considered as temporal dependence. In addition, geometry degradation of the central segment is also impacted by the surrounding segments and substructure conditions. Therefore, spatial dependency should be considered for adjacent segments. CNN-LSTM uniquely accounts for both spatial and temporal dependence in track geometry prediction and thus achieves superior performance.

Fig. 12(a) compares the predicted track geometry (partial of test dataset) one month in advance with the actual geometry measurement in the time domain. Fig. 12(b) presents the statistical distribution of the difference between the actual and predicted geometry amplitude. It indicates that the proposed model can provide an accurate prediction of geometry measurements. The error of the predicted results is symmetrically distributed, the mean error is approximately 0, and the standard deviation is 0.019.

Finally, the proposed model is applied to predict track geometry in two years (blind prediction) in support of predictive maintenance and capital planning. The trajectory of the geometry degradation (without intervention) over a short segment is presented in Fig. 13, where each line shows the trajectory of geometry degradation of a one-foot track segment. This indicates that track geometry at different locations has various degradation rates. Using the proposed model, track segments with faster degradation rates might be prioritized for maintenance activities.

6. Conclusion and discussion

6.1. Conclusion

Foot-by-foot track geometry prediction can be used to support maintenance tasks and capital planning and to enhance rail transportation safety by identifying track segments that are prone to track geometry defects. Highly accurate position information is a prerequisite for foot-by-foot geometry prediction. Therefore, this paper first proposes methods for correcting the relative positional error between different geometry measurements. Issues (i.e., rail side confusion and sign contradiction) associated with inspection vehicles moving in different directions are handled prior to estimating the positional error. The proposed positional error correction method is able to reduce the relative positional error to less than 1 foot with 99 % confidence interval, and thus supports foot-by-foot track geometry prediction.

Based on the processed geometry data and other related data (i.e., traffic, speed, grade, and curvature), the CNN-LSTM model is proposed to predict foot-by-foot track geometry measurements with consideration of spatial–temporal dependence. Specifically, CNN is applied to capture the spatial dependence by considering the surrounding conditions of central segments. LSTM is applied to capture the temporal dependence by learning the dynamic changes of geometry measurements. Our proposed CNN-LSTM model outperforms four other models, including the naïve model, MLP, plain CNN, and plain LSTM, in both short-term and long-term prediction. Finally, multi-step prediction is applied to provide the trajectory of geometry degradation over a long period in support of predictive maintenance and capital planning.

6.2. Discussion

This section discusses the limitations of current research and directions for future research. In data cleaning, current research applies threshold-based outlier detection approach to identify outliers in track geometry measurements. Nevertheless, this may cause misclassification

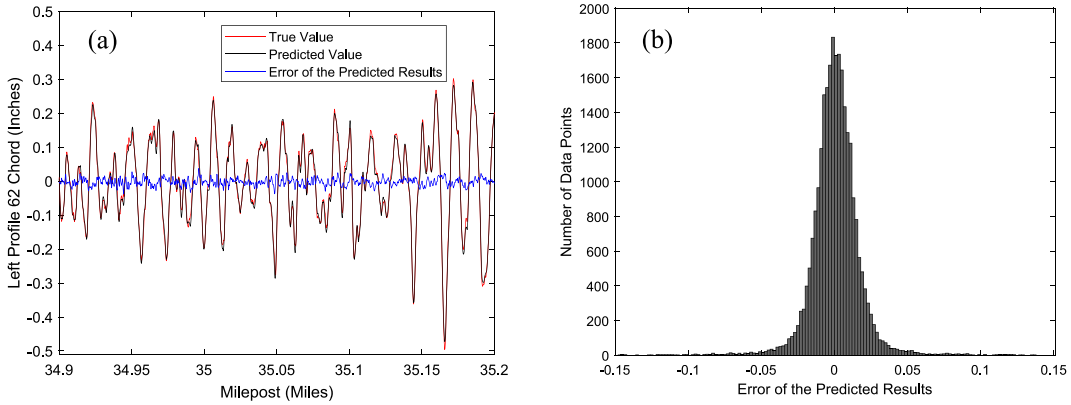

Fig. 12. CNN-LSTM Model for Predicting Track Geometry for One Month in Advance (a). Track Geometry Amplitudes; (b). Histogram of the Prediction Errors.

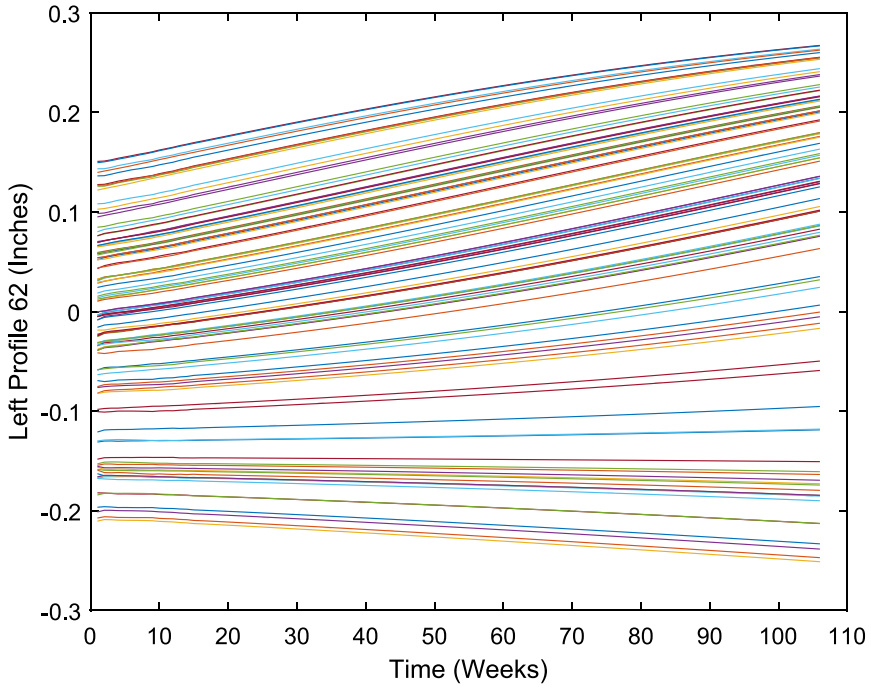

Fig. 13. Trajectory of Geometry Degradation for Two Years (Each Line Represents a One-Foot Track Segment).

in particular track sections (e.g., bridge–embankment transition zones) with large amplitude change due to the change of track stiffness. To this end, alternative outlier detection techniques based on characteristics of historical measurements may be considered in future research, which could provide a more robust solution for identifying outliers in geometry measurements.

Secondly, more geometry data could be collected to validate the performance of the proposed model at geometry prediction over a longer timespan. The current model can provide the trajectory of geometry degradation over a long period; however, the accuracy of the model decreases for long-term predictions. Therefore, in future research, it is essential to quantitively evaluate the accuracy of the model when applying it for long-term predictions.

Furthermore, it is important to optimize and improve the performance of the current prediction model, especially for long-term predictions. The first way to do so would be to consider more historical geometry measurements in the model, which would allow the model to learn the deterioration pattern of geometry from more historical measurements. An alternative solution would be to collect more factors related to the deterioration of track geometry to improve the performance of the model. Substructure and weather conditions (e.g., season, temperature, and precipitation) can affect the deterioration of track geometry. For example, track segments in highly fouled areas (greater ballast fouling index) are more likely to have a faster rate of geometry deterioration. Additionally, considering the influence of maintenance activities on the deterioration process, especially for long-term predictions (e.g., annual predictions), will further refine the model's predictions. Therefore, data with longer timespans and more influencing factors should be included in the model to contribute to better results in long-term geometry predictions, which ultimately supports better decision-making for railroad infrastructure maintenance and planning.

Lastly, the proposed methodology that combines a CNN-LSTM model for spatial and temporal dependence modeling has promising applications and scalability potential in various engineering domains, especially those dealing with time-series data and spatially correlated features. CNN considers the spatial correlation of data by conducting convolution operations. LSTM is able to capture the long-term dependence in the data by incorporating memory blocks to avoid vanishing and exploding gradient. Therefore, the proposed methodology could also be applied to infrastructure degradation such as highways by indicating locations susceptible to fatigue cracking and corrosion under both spatial and temporal influence. In addition to linear assets, the proposed methodology can be utilized to analyze complex systems by effectively extracting spatial and temporal features from data. For example, it can be employed to predict the behavior of traffic flow and weather systems as the CNN and LSTM can extract information from adjacent areas and historical records.

Declaration of Competing Interest

The authors declare that they have no known competing financial interests or personal relationships that could have appeared to influence the work reported in this paper. Part of this research was conducted when the corresponding author was at Rutgers Center for Advanced Infrastructure and Transportation (CAIT). However, the authors are solely responsible for all the views and analyses presented in this paper.

Data availability

Data will not be available due to a non-disclosure agreement with the data provider.

References

[1] R. Mohammadi, Q. He, F. Ghofrani, A. Pathak, A. Aref, Exploring the impact of foot-by-foot track geometry on the occurrence of rail defects, Transport. Res Part c: Emerg. Technol. 102 (2019) 153–172, https://doi.org/10.1016/j.trc.2019.03.004.
[2] S. Sharma, Y. Cui, Q. He, R. Mohammadi, Z. Li, Data-driven optimization of railway maintenance for track geometry, Transport. Res Part c: Emerg. Technol. 90 (2018) 34–58, https://doi.org/10.1016/j.trc.2018.02.019.
[3] X. Liu, M.R. Saat, C.P.L. Barkan, Analysis of causes of major train derailment and their effect on accident rates, Transp. Res. Rec. 2289 (2012) 154–163, https://doi.org/10.3141/2289-20.
[4] Federal Railroad Administration (FRA), Exhibit A: Autonomous track assessment cars (ATACs) characteristics, (2020). https://www.regulations.gov/document/FRA-2020-0013-0002 (accessed January 17, 2023).
[5] F. Ghofrani, Q. He, R.M.P. Goverde, X. Liu, Recent applications of big data analytics in railway transportation systems: A survey, Transport. Res Part c: Emerg. Technol. 90 (2018) 226–246, https://doi.org/10.1016/j.trc.2018.03.010.

[6] A.M. Zarembski, D. Einbinder, N. Attoh-Okine, Using multiple adaptive regression to address the impact of track geometry on development of rail defects, Constr. Build. Mater. 127 (2016) 546–555, https://doi.org/10.1016/j.conbuildmat.2016.10.012.

[7] M. Khosravi, I. Soleimanmeigouni, A. Ahmadi, A. Nissen, Reducing the positional errors of railway track geometry measurements using alignment methods: A comparative case study, Measurement 178 (2021), 109383, https://doi.org/10.1016/j.measurement.2021.109383.

[8] Y. Wang, P. Wang, X. Wang, X. Liu, Position synchronization for track geometry inspection data via big-data fusion and incremental learning, Transport. Res Part c: Emerg. Technol. 93 (2018) 544–565.

[9] I. Cárdenas-Gallo, C.A. Sarmiento, G.A. Morales, M.A. Bolivar, R. Akhavan-Tabatabaei, An ensemble classifier to predict track geometry degradation, Reliab. Eng. Syst. Saf. 161 (2017) 53–60, https://doi.org/10.1016/j.ress.2016.12.012.

[10] X. Wang, X. Liu, Z. Bian, A machine learning based methodology for broken rail prediction on freight railroads: A case study in the United States, Constr. Build. Mater. 346 (2022), 128353, https://doi.org/10.1016/j.conbuildmat.2022.128353.

[11] C. Higgins, X. Liu, Modeling of track geometry degradation and decisions on safety and maintenance: A literature review and possible future research directions, Proc. Institut. Mech. Eng. Part F: J. Rail Rapid Transit. 232 (2018) 1385–1397, https://doi.org/10.1177/0954409717721870.

[12] Y. Wang, P. Wang, H. Tang, X. Liu, J. Xu, J. Xiao, J. Wu, Assessment and prediction of high speed railway bridge long-term deformation based on track geometry inspection big data, Mech. Syst. Sig. Process. 158 (2021), 107749.

[13] A. Hamid, A. Gross, Track-quality indices and track degradation models for maintenance-of-way planning, Transp. Res. Board 802 (1981) 2–8.

[14] Y. Shafahi, P. Masoudi, R. Hakhamaneshi, Track degradation prediction models, using Markov Chain, artificial neural and neuro-fuzzy network, in: 8th World Congress on Railway Research, 2008: pp. 1–9.

[15] C. Hu, X. Liu, Modeling track geometry degradation using support vector machine technique, in: ASME/IEEE Joint Rail Conference, American Society of Mechanical Engineers, 2016, p. V001T01A011, doi: 10.1115/JRC2016-5739.

[16] J.S. Lee, S.H. Hwang, I.Y. Choi, I.K. Kim, Prediction of track deterioration using maintenance data and machine learning schemes, J. Transport. Eng. Part a: Syst. 144 (2018) 04018045, https://doi.org/10.1061/JTEPBS.0000173.

[17] S. Goodarzi, H.F. Kashani, J. Oke, C.L. Ho, Data-driven methods to predict track degradation: A case study, Constr. Build. Mater. 344 (2022), 128166, https://doi.org/10.1016/j.conbuildmat.2022.128166.

[18] Q. He, H. Li, D. Bhattacharjya, D.P. Parikh, A. Hampapur, Track geometry defect rectification based on track deterioration modelling and derailment risk assessment, J. Oper. Res. Soc. 66 (2015) 392–404, https://doi.org/10.1057/jors.2014.7.

[19] X. Wang, X. Liu, T.L. Euston, Relationship between track geometry defect occurrence and substructure condition: A case study on one passenger railroad in the United States, Constr. Build. Mater. 365 (2023), 130066, https://doi.org/10.1016/j.conbuildmat.2022.130066.

[20] G. Shen, R. Ding, M. Yang, D. Han, B. Zhang, An elastic manifold learning approach to beat-to-beat interval estimation with ballistocardiography signals, Adv. Eng. Inf. 44 (2020), 101051, https://doi.org/10.1016/j.aei.2020.101051.

[21] J. Yang, T. Cheng, J. Teizer, P.A. Vela, Z.K. Shi, A performance evaluation of vision and radio frequency tracking methods for interacting workforce, Adv. Eng. Inf. 25 (2011) 736–747, https://doi.org/10.1016/j.aei.2011.04.001.

[22] B. Allotta, V. Colla, M. Malvezzi, Train position and speed estimation using wheel velocity measurements, Proc. Institut. Mech. Eng. Part F: J. Rail Rapid Transit. 216 (2002) 207–225, https://doi.org/10.1243/095440902760213639.

[23] M. Chen, Y. Sun, Y. Guo, W. Zhai, Study on effect of wheel polygonal wear on high-speed vehicle-track-subgrade vertical interactions, Wear 432–433 (2019), 102914, https://doi.org/10.1016/j.wear.2019.05.029.

[24] I. Hussain, T.X. Mei, R.T. Ritchings, Estimation of wheel–rail contact conditions and adhesion using the multiple model approach, Veh. Syst. Dyn. 51 (2013) 32–53, https://doi.org/10.1080/00423114.2012.708759.

[25] H. Mori, H. Tsunashima, T. Kojima, A. Matsumoto, T. Mizuma, Condition monitoring of railway track using in-service vehicle, J. Mech. Syst. Transport. Logist. 3 (2010) 154–165, https://doi.org/10.1299/jmtl.3.154.

[26] C. Specht, W. Koc, P. Chrostowski, J. Szmaglinski, The analysis of tram tracks geometric layout based on mobile satellite measurements, Urban Rail Transit 3 (2017) 214–226, https://doi.org/10.1007/s40864-017-0071-3.

[27] P. Xu, Q. Sun, R. Liu, R.R. Souleyrette, Optimal match method for milepoint postprocessing of track condition data from subway track geometry cars, J. Transp. Eng. 142 (2016) 04016028, https://doi.org/10.1061/(ASCE)TE.1943-5436.0000859.

[28] S.S. Saab, A map matching approach for train positioning. I. Development and analysis, IEEE Trans. Veh. Technol. 49 (2000) 467–475, https://doi.org/10.1109/25.832978.

[29] S.S. Saab, A map matching approach for train positioning. II. Application and experimentation, IEEE Trans. Veh. Technol. 49 (2000) 476–484, https://doi.org/10.1109/25.832979.

[30] A.J.D. Santos, A.R. Soares, F.M. de Almeida Redondo, N.B. Carvalho, Tracking trains via radio frequency systems, IEEE Trans. Intell. Transp. Syst. 6 (2005) 244–258, https://doi.org/10.1109/TITS.2005.848369.

[31] Y. Wang, J. Cong, P. Wang, X. Liu, H. Tang, A data-fusion approach for speed estimation and location calibration of a metro train based on low-cost sensors in smartphones, IEEE Sens. J. 19 (2019) 10744–10752, https://doi.org/10.1109/JSEN.2019.2933638.

[32] W. Hanreich, P. Mittermayr, G. Presle, Track geometry measurement database and calculation of equivalent conicities of the OBB network, in: American Railway Engineering and Maintenance of Way Association 2002 Conference, Washington DC, 2002.

[33] A. Yang, Automatic correct milepost system of geometry inspection car based on RFID, Railway Comput. Applicat. 18 (2009) 39–41.

[34] P. Xu, Q.-X. Sun, R.-K. Liu, F.-T. Wang, Key equipment identification model for correcting milepost errors of track geometry data from track inspection cars, Transport. Res. Part c: Emerg. Technol. 35 (2013) 85–103, https://doi.org/10.1016/j.trc.2013.06.006.

[35] H. Li, Y. Xu, A method to correct the mileage error in railway track geometry data and its usage, Traffic Transport. Stud. 2010 (2010) 1130–1135.

[36] G. Sui, H. Li, Y. Xu, Mileage calibration algorithm of track geometry data, J. Transp. Informat. Safety 27 (2009) 18–21.

[37] E.T. Selig, G.M. Cardillo, E. Stephens, A. Smith, Analyzing and forecasting railway data using linear data analysis, WIT Trans. Built Environ. 103 (2008) 25–34.

[38] P. Xu, R. Liu, Q. Sun, L. Jiang, Dynamic-time-warping-based measurement data alignment model for condition-based railroad track maintenance, IEEE Trans. Intell. Transp. Syst. 16 (2014) 799–812.

[39] H. Sakoe, S. Chiba, Dynamic programming algorithm optimization for spoken word recognition, IEEE Trans. Acoust. Speech Signal Process. 26 (1978) 43–49, https://doi.org/10.1109/TASSP.1978.1163055.

[40] N.-P.-V. Nielsen, J.M. Carstensen, J. Smedsgaard, Aligning of single and multiple wavelength chromatographic profiles for chemometric data analysis using correlation optimised warping, J. Chromatogr. A 805 (1998) 17–35, https://doi.org/10.1016/S0021-9673(98)00021-1.

[41] J.T.W.E. Vogels, A.C. Tas, J. Venekamp, J. Van Der Greef, Partial linear fit: A new NMR spectroscopy preprocessing tool for pattern recognition applications, J. Chemom. 10 (1996) 425–438, https://doi.org/10.1002/(SICI)1099-128X(199609)10:5/6<425::AID-CEM442>3.0.CO;2-S.

[42] F. Savorani, G. Tomasi, S.B. Engelsen, icoshift: A versatile tool for the rapid alignment of 1D NMR spectra, J. Magn. Reson. 202 (2010) 190–202, https://doi.org/10.1016/j.jmr.2009.11.012.

[43] J.W.H. Wong, C. Durante, H.M. Cartwright, Application of Fast Fourier Transform cross-correlation for the alignment of large chromatographic and spectral datasets, Anal. Chem. 77 (2005) 5655–5661, https://doi.org/10.1021/ac050619p.

[44] T.N. Vu, D. Valkenborg, K. Smets, K.A. Verwaest, R. Dommisse, F. Lemière, A. Verschoren, B. Goethals, K. Laukens, An integrated workflow for robust alignment and simplified quantitative analysis of NMR spectrometry data, BMC Bioinf. 12 (2011) 405, https://doi.org/10.1186/1471-2105-12-405.

[45] K.A. Veselkov, J.C. Lindon, T.M.D. Ebbels, D. Crockford, V.V. Volynkin, E. Holmes, D.B. Davies, J.K. Nicholson, Recursive segment-wise peak alignment of biological ^{1}h NMR spectra for improved metabolic biomarker recovery, Anal. Chem. 81 (2009) 56–66, https://doi.org/10.1021/ac8011544.

[46] N. Davari, B. Veloso, G.D.A. Costa, P.M. Pereira, R.P. Ribeiro, J. Gama, A survey on data-driven predictive maintenance for the railway industry, Sensors 21 (2021) 5739, https://doi.org/10.3390/s21175739.

[47] M. Binder, V. Mezhuyev, M. Tschandl, Predictive maintenance for railway domain: a systematic literature review, IEEE Eng. Manag. Rev. 51 (2023) 120–140, https://doi.org/10.1109/EMR.2023.3262282.

[48] L.F. Caetano, P.F. Teixeira, Predictive maintenance model for ballast tamping, J. Transp. Eng. 142 (2016) 04016006, https://doi.org/10.1061/(ASCE)TE.1943-5436.0000825.

[49] H. Chang, R. Liu, Q. Li, A multi-stage linear prediction model for the irregularity of the longitudinal level over unit railway sections, WIT Trans. Built Environ. 114 (2010) 641–650.

[50] R. Liu, P. Xu, F. Wang, Research on a short-range prediction model for track irregularity over small track lengths, J. Transp. Eng. 136 (2010) 1085–1091, https://doi.org/10.1061/(ASCE)TE.1943-5436.0000192.

[51] P. Xu, Q. Sun, R. Liu, F. Wang, A short-range prediction model for track quality index, Proc. Institut. Mech. Eng. Part F: J. Rail Rapid Transit. 225 (2011) 277–285, https://doi.org/10.1177/2041301710392477.

[52] J. Ding, L. Han, X. Chen, Time series AR modeling with missing observations based on the polynomial transformation, Math. Comput. Model. 51 (2010) 527–536, https://doi.org/10.1016/j.mcm.2009.11.016.

[53] J. Chaolong, X. Weixiang, W. Futian, W. Hanning, Track irregularity time series analysis and trend forecasting, Discret. Dyn. Nat. Soc. 2012 (2012) 1–15, https://doi.org/10.1155/2012/387857.

[54] M. Zhu, X. Cheng, L. Miao, X. Sun, S. Wang, Advanced stochastic modeling of railway track irregularities, Adv. Mech. Eng. 5 (2013), 401637, https://doi.org/10.1155/2013/401637.

[55] C. Meier-Hirmer, G. Riboulet, F. Sourget, M. Roussignol, Maintenance optimization for a system with a gamma deterioration process and intervention delay: Application to track maintenance, Proc. Instit. Mech. Eng. Part o: J. Risk Reliab. 223 (2009) 189–198, https://doi.org/10.1243/1748006XJRR234.

[56] L. Bai, R. Liu, Q. Sun, F. Wang, P. Xu, Markov-based model for the prediction of railway track irregularities, Proc. Institut. Mech. Eng. Part F: J. Rail Rapid Transit. 229 (2015) 150–159, https://doi.org/10.1177/0954409713503460.

[57] Q. He, H. Li, D. Bhattacharjya, D.P. Parikh, A. Hampapur, Railway track geometry defect modeling: deterioration, derailment risk and optimal repair, in: Proceedings of the Transportation Research Board Annual Meeting, The Academy of Transportation Research Board, 2013.

[58] A. Falamarzi, S. Moridpour, M. Nazem, S. Cheraghi, Development of random forests regression model to predict track degradation index: Melbourne case study, in: Australian Transport Research Forum, 2018: p. 12.

[59] A. Lasisi, N. Attoh-Okine, Principal components analysis and track quality index: A machine learning approach, Transport. Res. Part c: Emerg. Technol.. 91 (2018) 230–248, https://doi.org/10.1016/j.trc.2018.04.001.

[60] F. Rosenblatt, Principles of neurodynamics. perceptrons and the theory of brain mechanisms, Cornell Aeronautical Lab Inc Buffalo NY, 1961.
[61] H. Khajehei, A. Ahmadi, I. Soleimanmeigouni, M. Haddadzade, A. Nissen, M. J. Latifi Jebelli, Prediction of track geometry degradation using artificial neural network: a case study, Int. J. Rail Transport. 10 (2022) 24–43, https://doi.org/10.1080/23248378.2021.1875065.
[62] A. Falamarzi, S. Moridpour, M. Nazem, Development of a tram track degradation prediction model based on the acceleration data, Struct. Infrastruct. Eng. 15 (2019) 1308–1318, https://doi.org/10.1080/15732479.2019.1615963.
[63] J. Deng, W. Dong, R. Socher, L.-J. Li, K. Li, L.i. Fei-Fei, ImageNet: A large-scale hierarchical image database, in: 2009 IEEE Conference on Computer Vision and Pattern Recognition, IEEE, Miami, FL, 2009, pp. 248–255, https://doi.org/10.1109/CVPR.2009.5206848.
[64] O. Abdel-Hamid, A. Mohamed, H. Jiang, L. Deng, G. Penn, D. Yu, Convolutional neural networks for speech recognition, IEEE/ACM Trans. Audio Speech Lang. Process. 22 (2014) 1533–1545, https://doi.org/10.1109/TASLP.2014.2339736.
[65] J. Wang, L.-C. Yu, K.R. Lai, X. Zhang, Tree-Structured regional CNN-LSTM model for dimensional sentiment analysis, IEEE/ACM Trans. Audio Speech Lang. Process. 28 (2020) 581–591, https://doi.org/10.1109/TASLP.2019.2959251.
[66] F. Burden, D. Winkler, Bayesian regularization of neural networks, in: D. J. Livingstone (Ed.), Artificial Neural Networks, Humana Press, Totowa, NJ, 2008, pp. 23–42, https://doi.org/10.1007/978-1-60327-101-1_3.
[67] T. de Bruin, K. Verbert, R. Babuska, Railway track circuit fault diagnosis using recurrent neural networks, IEEE Trans. Neural Networks Learn. Syst. 28 (2017) 523–533, https://doi.org/10.1109/TNNLS.2016.2551940.
[68] M. Heidarysafa, K. Kowsari, L. Barnes, D. Brown, Analysis of railway accidents' narratives using deep learning, in: 2018 17th IEEE International Conference on Machine Learning and Applications (ICMLA), IEEE, Orlando, FL, 2018, pp. 1446–1453, https://doi.org/10.1109/ICMLA.2018.00235.
[69] L. Zhao, Y. Song, C. Zhang, Y. Liu, P. Wang, T. Lin, M. Deng, H. Li, T-GCN: A temporal graph convolutional network for traffic prediction, IEEE Trans. Intell. Transport. Syst. 21 (2020) 3848–3858, https://doi.org/10.1109/TITS.2019.2935152.
[70] Y. Hu, C. Xia, J. Chen, X. Gao, Clash context representation and change component prediction based on graph convolutional network in MEP disciplines, Adv. Eng. Inf. 55 (2023), 101896, https://doi.org/10.1016/j.aei.2023.101896.
[71] S. Ma, L. Gao, X. Liu, J. Lin, Deep learning for track quality evaluation of high-speed railway based on vehicle-body vibration prediction, IEEE Access 7 (2019) 185099–185107, https://doi.org/10.1109/ACCESS.2019.2960537.
[72] Y.-C. Chi, H.-C. Wang, Establish a patent risk prediction model for emerging technologies using deep learning and data augmentation, Adv. Eng. Inf. 52 (2022), 101509, https://doi.org/10.1016/j.aei.2021.101509.
[73] S. Zhou, S. Thomas Ng, G. Huang, J. Dao, D. Li, Extracting interrelated information from road-related social media data, Adv. Eng. Inf. 54 (2022), 101780, https://doi.org/10.1016/j.aei.2022.101780.
[74] Y. Bengio, P. Simard, P. Frasconi, Learning long-term dependencies with gradient descent is difficult, IEEE Trans. Neural Netw. 5 (1994) 157–166, https://doi.org/10.1109/72.279181.
[75] S. Hochreiter, J. Schmidhuber, Long short-term memory, Neural Comput. 9 (1997) 1735–1780, https://doi.org/10.1162/neco.1997.9.8.1735.
[76] J.F. Kolen, S.C. Kremer, Gradient flow in recurrent nets: The difficulty of learning long-term dependencies, in: A Field Guide to Dynamical Recurrent Networks, 2001: pp. 237–243. Doi: 10.1109/9780470544037.ch14.
[77] A. Zhang, Z.C. Lipton, M. Li, A.J. Smola, Dive into deep learning, 2021, doi: 10.48550/ARXIV.2106.11342.
[78] A. de Myttenaere, B. Golden, B. Le Grand, F. Rossi, Mean absolute percentage error for regression models, Neurocomputing 192 (2016) 38–48, https://doi.org/10.1016/j.neucom.2015.12.114.